

Nonlinear optical properties of 2D- $W_xMo_{1-x}Te_2$ and its applications in energy conversion and storage devices

Mohsen Jemai¹, Nouha Mastour², Said Ridene³

Advanced Materials and Quantum Phenomena Laboratory,

Physics Department, Sciences Faculty of Tunis,

Tunis El Manar University, 2092 Tunis, Tunisia.

[1mohsen.jemai@fst.utm.tn](mailto:mohsen.jemai@fst.utm.tn)

[2mohsen.jemai@fst.utm.tn](mailto:mohsen.jemai@fst.utm.tn)

[3said.ridene@fst.utm.tn](mailto:said.ridene@fst.utm.tn)

Abstract— Linear and nonlinear absorption coefficients (LNACs) and refractive index (RIs) in $W_xMo_{1-x}Te_2$ are investigated using 2D-hamiltonian and compact density matrix approach taking into account on the W-concentrations. The results suggest that individual $MoTe_2$, WTe_2 have high absorption in some portions of the visible region (630 and 800 nm) and in the near infrared region. The absorption coefficient is seen to increase with the wavelength and appears to be shifted towards the red end of the spectrum. High absorption is also observed in the entire visible region (630 to 780 nm) of the spectrum for all W-concentration. Furthermore, it is observed that the monolayer of $W_xMo_{1-x}Te_2$ is beneficial in energy storage and for solar energy conversion.

Keywords— Linear and nonlinear ACs, RIs, $W_xMo_{1-x}Te_2$, W-concentration effect

I. INTRODUCTION

Monolayers and few-layer of transition metal dichalcogenides MX_2 (M=Mo or W, X=S, Te, or Se) are of great interest for their exceptional optical and electronic properties. Indeed, $MoTe_2$, WTe_2 and their $W_xMo_{1-x}Te_2$ alloys, are considered as the best promising materials from this MX_2 groups by their spectacular physicochemical properties [1]-[7]. In fact $W_xMo_{1-x}Te_2$ alloys will have in the future potential applications such as green energy due to their non-toxicity and their significant stability [6]-[8]. Their direct band gap allows many investigations by electric and magneto-optical techniques [9], [10]. Especially, two-dimensional $W_xMo_{1-x}Te_2$ ternary alloys show important proprieties for many applications compared to $MoTe_2$ or WTe_2 pure [11], [12]. While there has been a tremendous progress in the synthesis and optoelectronic characterization of 2D crystal alloys, little has been done to understand their atomic-scale alloy structure [13], [14]. From a nano-electronics and optoelectronics point of view, recent experimental work has been proposed for $W_xMo_{1-x}Te_2$ two-dimensional direct-gap semiconductors in a new type of field-effect transistors with extinction rates high [15], as well as in devices such as phototransistors, memories and sensors [16], [17]. Main focal points associated with $W_xMo_{1-x}Te_2$ ternary alloys are their larger AC and RRIC and binding exciton energy [14], [18]. In addition, the incorporation of a small concentration of tungsten (W) with molybdenum and sulfur elements can introduce a significant reduction in the band gap which can be beneficial for potential applications in mid-infrared devices. Several reports in the context of $W_xMo_{1-x}Te_2$ monolayers are reported [11]-[14], [18], however its response on the electric and magneto-optical properties has hitherto not been reported. Indeed the consideration of linear and nonlinear electric and magneto-optical ACs and RICs in $W_xMo_{1-x}Te_2$ ternary alloys and the role of W-contents are still lacking. In this work, we investigate the effect of electric, magneto-optical, W-contents on the linear and nonlinear optical properties of $W_xMo_{1-x}Te_2$ alloys. We have reported the optical performance of this alloy in order to prove that $W_xMo_{1-x}Te_2$ layered is promoter for potential application in optoelectronic devices. We have used compact density matrix to calculate the LNACs and RICs for inter-band transitions. Note that the theoretical model is already developed at zero temperature in refs.[19]-[21], we have estimated this theoretical study, from these references and also from our previous reports of the linear and nonlinear intra- and inter-bands optical absorptions of quantum well and 2D materials [22], [23]. Besides, in this work we have detailed and adapted this model for $W_xMo_{1-x}Te_2$ monolayer not only at zero temperature but for variable temperature and charge carrier's densities n_c and for studying the effects of both electric and magnetic fields. This theoretical insight has been chosen as an essential point in our study of the absorption coefficients and refractive index for the different tungsten concentration of $W_xMo_{1-x}Te_2$ structure.

We have organized the paper as follows: in section II, we present the theoretical and numerical methods, the results and discussion are detailed in section III and the conclusion is given in section IV.

II. THEORETICAL STUDY OF LINEAR AND NONLINEAR ELECTRIC AND MAGNETO-OPTICAL PROPERTIES OF MX_2

The linear and nonlinear optical properties of $\text{W}_x\text{Mo}_{1-x}\text{Te}_2$ have been studied with the theoretical model of compact density matrix. Thus, the ACs and RICs are calculated for MoTe_2 , WTe_2 and their alloys. The Hamiltonian describing the two-dimensional systems of type 2D- $\text{W}_x\text{Mo}_{1-x}\text{Te}_2$ is given by [20]:

$$\mathbf{H} = v_F(\boldsymbol{\tau}\sigma_x\pi_x + \sigma_y\pi_y) + (\boldsymbol{\Delta}_{\tau,s} + d.\boldsymbol{\Delta}_z)\sigma_z + \mathbf{O}_{\tau,s} + s\mathbf{M}_s - \boldsymbol{\tau}\mathbf{M}_v \quad (1)$$

where $\hbar v_F$ (eV.Å) that correspond to the Fermi energy ($E_F = \hbar v_F \sqrt{\pi n_c}$ with $n_c = 1.35 \times 10^{13} \text{ cm}^{-2}$). σ_i ($i = x, y, z$) are the Pauli matrices, the valley index $\tau = \pm 1$ is for K and K' one, $s = \pm 1$ is for the spin up and spin down, $2d$ is the distance between the $\text{M} \equiv (\text{Mo or W})$ and Te sub-lattices, the electric field term is $\Delta_z = eE_z$, the quantity $\vec{\pi} = \vec{p} + e\vec{A}$ is the canonical momentum with \vec{p} being the normal momentum and $\vec{A} = (0, B.x, 0)$ being the vector potential in the Landau gauge. The Dirac mass and the offset energy are expressions as follows [21]:

$$\boldsymbol{\Delta}_{\tau,s} = \boldsymbol{\Delta} - s\boldsymbol{\tau}(\lambda_v - \lambda_c)/4 \quad \text{and} \quad \mathbf{O}_{\tau,s} = s\boldsymbol{\tau}(\lambda_v + \lambda_c)/4 \quad (2)$$

where $\boldsymbol{\Delta}$ is the intrinsic band-gap [20], $M_j = g_j \mu_B B/2$ the Zeeman fields with $j = s, v$ corresponding to the spin and valley ones, $\mu_B = e\hbar/2m_e$ is the Bohr magneton with $m^* = m_e/m_0$ being the electron effective mass in $\text{W}_x\text{Mo}_{1-x}\text{Te}_2$, and g_j ($j = s, v$) are the Landé factors [8]. The corresponding eigen-values of Eq. (1) are:

$$\varepsilon_\lambda = \varepsilon_{n,s}^{\tau,p} = \mathbf{p}\boldsymbol{\varepsilon}_{n,s}^\tau + \mathbf{O}_{\tau,s} + s\mathbf{M}_s - \boldsymbol{\tau}\mathbf{M}_v \quad (3)$$

In Eq. (3), the index $p = \pm 1$ refers to the conduction and valence bands, and

$$\boldsymbol{\varepsilon}_{n,s}^\tau = \sqrt{n(\hbar\omega_c)^2 + (\boldsymbol{\Delta}_{\tau,s}^z)^2}. \quad (4)$$

We have denoted $\boldsymbol{\Delta}_{\tau,s}^z = \boldsymbol{\Delta}_{\tau,s} + d.\boldsymbol{\Delta}_z$ referring to the effective Dirac mass term and $\omega_c = \sqrt{2}v_F/\ell_B$ is the cyclotron frequency ($\ell_B = \sqrt{\hbar/(eB)}$ is the magnetic length). The eigenfunction corresponding to the Hamiltonian given in Eq. (1) are:

$$|\lambda\rangle = |\mathbf{n}, s; \boldsymbol{\tau}, p\rangle = \frac{1}{\sqrt{L_y}} e^{ik.y} \boldsymbol{\psi}_{n,s}^{\tau,p}(x) \quad \text{with} \quad \boldsymbol{\psi}_{n,s}^{\tau,p}(x) = \begin{pmatrix} \boldsymbol{\tau} A_{n,s}^{\tau,p} \Phi_{n-1}(x-x_0) \\ B_{n,s}^{\tau,p} \Phi_n(x-x_0) \end{pmatrix} \quad (5)$$

and $\Phi_n(x-x_0) = \exp[-C(x-x_0)^2/2] H_n[C(x-x_0)]$ are the normalization oscillator functions centered at $x_0 = \ell_B^2 k$ (with $C = m_e \omega_c / \hbar$ and $H(x)$ is Hermite polynomial), and the normalization constants are:

$$A_{n,s}^{\tau,p} = \sqrt{\frac{1}{2} + \frac{\boldsymbol{\Delta}_{\tau,s}^z}{p\varepsilon_{n,s}^\tau}}, \quad B_{n,s}^{\tau,p} = \sqrt{\frac{1}{2} - \frac{\boldsymbol{\Delta}_{\tau,s}^z}{p\varepsilon_{n,s}^\tau}}. \quad (6)$$

In the next, we will use the above equations to evaluate the magneto-optical ACs and RI changes in $\text{W}_x\text{Mo}_{1-x}\text{Te}_2$ monolayer. Using the compact density matrix approach, the linear and nonlinear optical susceptibilities for transitions between the two bands $|\lambda\rangle$ and $|\lambda'\rangle$ can be calculated as follows [19]:

$$\chi_{xx}^{(1)}(\omega) = \frac{n_c}{2\pi\varepsilon_0\hbar\ell_B^2} \sum_{\lambda,\lambda'} \frac{[f(\varepsilon_\lambda) - f(\varepsilon_{\lambda'})](d_{\lambda'\lambda}^x)^* d_{\lambda\lambda'}^x}{\varepsilon_{\lambda'} - \varepsilon_\lambda - \hbar\omega - i\hbar\gamma_0} \quad (7)$$

$$\chi_{xx}^{(3)}(\omega) = \frac{n_c|E|^2}{2\pi\varepsilon_0\hbar\ell_B^2} \sum_{\lambda,\lambda'} \frac{[f(\varepsilon_\lambda) - f(\varepsilon_{\lambda'})](d_{\lambda'\lambda}^x)^* d_{\lambda\lambda'}^x}{\varepsilon_{\lambda'} - \varepsilon_\lambda - \hbar\omega - i\hbar\gamma_0} \left[\frac{4(d_{\lambda'\lambda}^x)^* d_{\lambda\lambda'}^x}{[\varepsilon_{\lambda'} - \varepsilon_\lambda - \hbar\omega]^2 + (\hbar\gamma_0)^2} - \frac{[d_{\lambda'\lambda'}^x - d_{\lambda\lambda}^x]^2}{[\varepsilon_{\lambda'} - \varepsilon_\lambda - i\hbar\gamma_0][\varepsilon_{\lambda'} - \varepsilon_\lambda - \hbar\omega - i\hbar\gamma_0]} \right] \quad (8)$$

where h (Å) is the thickness of the monolayer MTe_2 ($\text{M} \equiv \text{Mo or W}$), $\hbar\omega$ is the photon energy, $\hbar\gamma_0 = 0.2\sqrt{B}$ (meV) [19] and $f(E)$ is the Fermi-Dirac distribution at a temperature T . $d_{\lambda'\lambda}^x$ is the dipole matrix element in the x -direction, which is given as follows :

$$d_{\lambda'\lambda}^x = -e\langle n', s'; \tau', p' | x | n, s; \tau, p \rangle \delta_{kk'} = ie\tau \frac{\hbar v_F}{\varepsilon_{\lambda'} - \varepsilon_{\lambda}} [\tau' (A_{n',s'}^{\tau',p'})^* B_{n,s}^{\tau,p} + \tau (B_{n',s'}^{\tau',p'})^* A_{n,s}^{\tau,p}] \delta_{kk'} \quad (9)$$

From the expressions for the optical susceptibilities shown in eq.(8), we can find the optical LNACs

$$\alpha(\omega, I) = \alpha^{(1)}(\omega) + \alpha^{(3)}(\omega, I) \quad \text{with} \quad \alpha^{(k)} = \frac{\omega}{c} \sqrt{\frac{\mu_r}{\varepsilon_r}} \text{Im}[\chi_{xx}^{(k)}] \quad (10)$$

where $k = 1, 3$ for the linear and nonlinear terms. The RIs changes as follows [24]

$$\Delta n(\omega, I) = \Delta n^{(1)}(\omega) + \Delta n^{(3)}(\omega, I) \quad \text{with} \quad \Delta n^{(k)} = \frac{1}{2n_r} \text{Re}[\chi_{xx}^{(k)}] \quad (11)$$

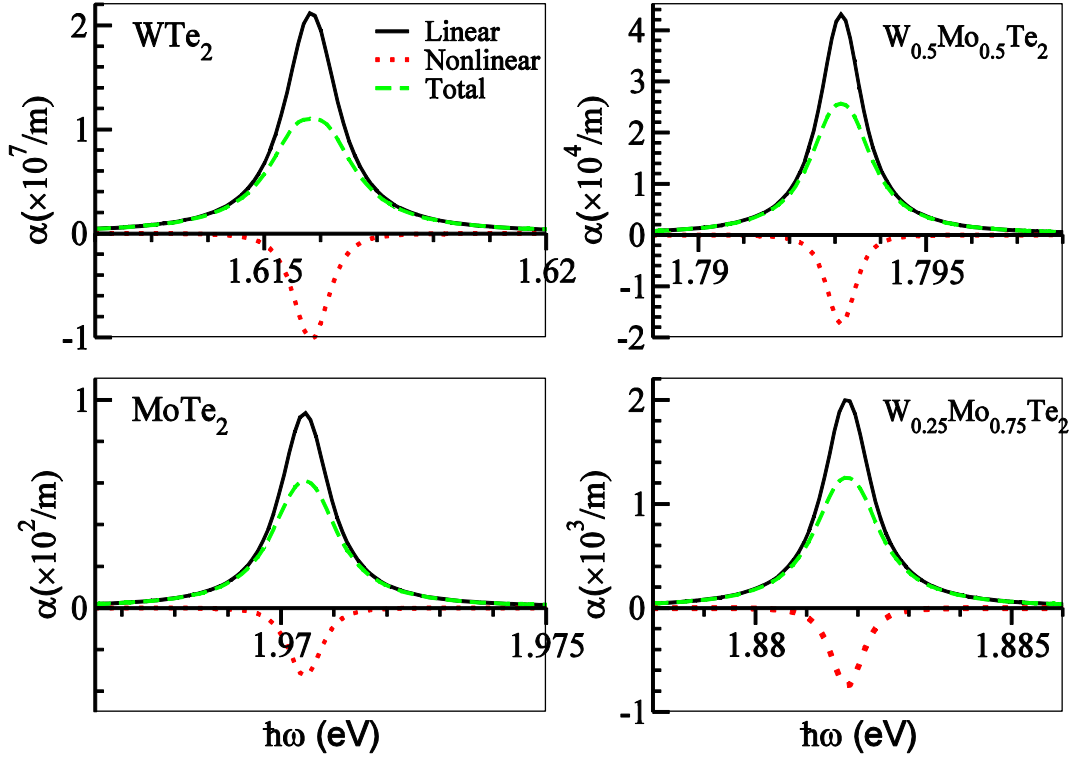


Fig. 1 Dependence on the photon energy of the linear, the third-order nonlinear ACs due to inter-band transitions for the optical phonon scattering for light intensity $I = 2.0 \times 10^6 \text{ W/m}^2$, magnetic field $B = 10 \text{ T}$, temperature $T = 300 \text{ K}$ and for different W-concentrations.

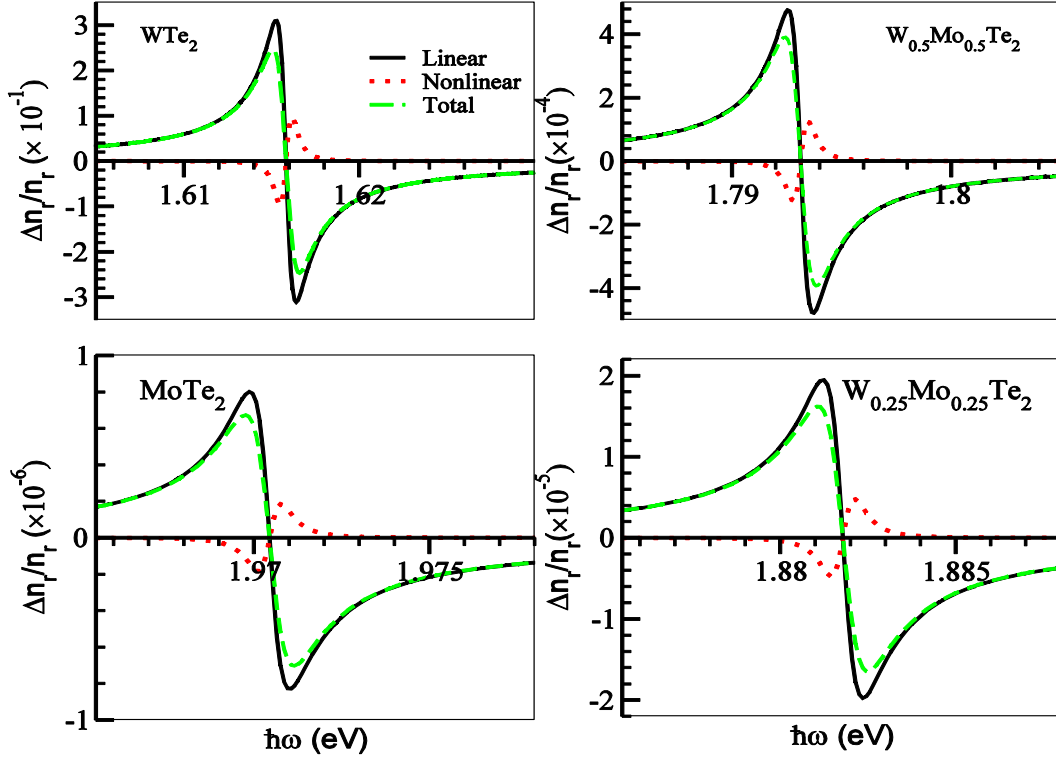


Fig. 2 Dependence on the photon energy of the linear, the third-order nonlinear RIs due to inter-band transitions for the optical phonon scattering for light intensity $I = 2.0 \times 10^6$ W/m², magnetic field $B = 10$ T, temperature $T = 300$ K and for different W-concentrations.

And $I = 2\varepsilon_0 n_r c |E|^2$ is the optical intensity of the incident photon which excites the system and leads to the optical transitions. $n_r = \sqrt{\varepsilon_r}$ being the refractive index of the MTe₂ ($M \equiv \text{Mo or W}$) material and μ_r the permeability of the material. We will only focus in the numerical evaluation of linear, nonlinear and the total LNACs and RICs in $W_x\text{Mo}_{1-x}\text{Te}_2$ monolayer. For the K valley (K and K' valleys are similar), we put $\tau = \tau' = 1$ in all calculations. The value of electric field is chosen to cancel the spin-orbit coupling term in the $K \uparrow$ and $K' \downarrow$ states as $d \cdot \Delta_z = (\lambda_v - \lambda_c)/4$. For the inter-band transitions, the absorbed photon energies are given by:

$$\hbar\omega_{\text{inter}} = \frac{(2n+1)\hbar\omega_c}{2[\Delta - s(\lambda_v - \lambda_c)/4 + d \cdot \Delta_z]} + 2[\Delta - s(\lambda_v - \lambda_c)/4 + d \cdot \Delta_z] \quad (12)$$

and it is proportional to the Landau level index, n . Therefore, we consider $n = 1$ and $\hbar\omega_{\text{inter}}$ is found to be proportional to 2Δ . It is important to note that, we have considered one-photon excitation because the two poles of the linear (Eq. 7) and nonlinear (Eq. 8) susceptibility functions are located at the same frequency.

III. RESULTS AND DISCUSSION

We begin our study by the calculation of LNACs and RICs due to the inter-band transition. All the parameters of MoTe₂ and WTe₂ are listed in Table I. We have used linear interpolation for $W_x\text{Mo}_{1-x}\text{Te}_2$ alloys. For the inter-band transitions, our calculation has been considered between the highest occupied valence and first conduction band-states. Figure 1 and 2 shows, the linear, the third-order nonlinear ACs and RICs due to inter-band transition for the optical phonon scattering, for light intensity $I = 2.0 \times 10^6$ W/m², magnetic field $B = 10$ T, temperature $T = 300$ K and for different W-concentration $x = 0.0, 0.25, 0.5$ and 1.0 of $W_x\text{Mo}_{1-x}\text{Te}_2$ monolayer.

The results are calculated for the spin-up, the spin-down states and as well as for their sum. With increase of W-concentration the peak positions give a red-shift for both LNACs and RICs and reduce in their amplitudes. The absorption factor decreases with a factor of 10^5 from $x = 1$ to $x = 0$. However, in order to maintain a high intensity of LNACs and RICs for the $W_x\text{Mo}_{1-x}\text{Te}_2$ alloys it is preferable to take a low W-concentration. It is important to note that the linear interpolation technique can be justified for the $W_x\text{Mo}_{1-x}\text{Te}_2$ structure due to the fact that the parameters of WTe₂ and MoTe₂ are very close (little difference between them, table I).

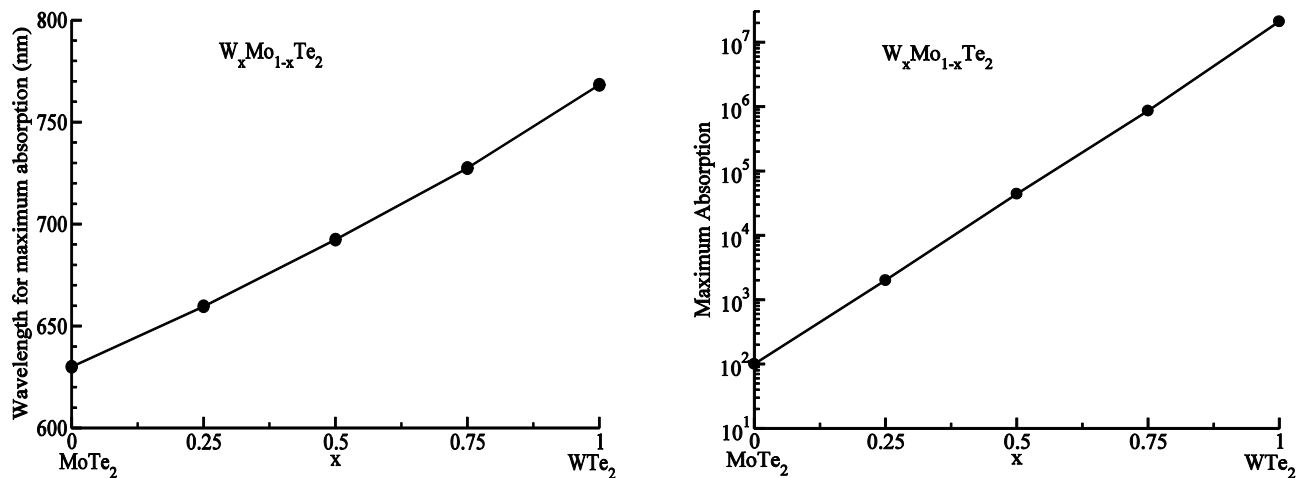


Fig. 3 Dependence of wavelength of maximum absorption as function of x for different W-concentrations in the monolayer $W_xMo_{1-x}Te_2$. Note that we use the same parameters as Fig. 1.

In addition, the obtained results show that the LNACs and RIC can be shifted from minimum to maximum red-band (630 – 760 nm) through varying the tungsten concentration (see Figs. 1, 2 and 3). However, the desired transition can be achieved by varying the tungsten concentration. This will be in good argument for the fabrication of samples with variable gaps [6], [7], otherwise, for the absorption or detection of light excitation and its applications in energy conversion and storage devices [8].

TABLE I

PARAMETERS USED IN THE CALCULATION FOR THE TWO TDMCs TAKEN FROM REF. [1-8]. THE % DIFF REPRESENTS THE PERCENTAGE DIFFERENCE BETWEEN THE PARAMETERS. FOR $W_xMo_{1-x}Te_2$, WE HAVE CONSIDERED THE INTERPOLATION FORM AS : $P_{W_xMo_{1-x}Te_2} = xP_{WTe_2} + (1-x)P_{MoTe_2}$.

Parameters	MoTe ₂	WTe ₂
$\hbar v_F$ (eV. Å)	3.06	2.1
Distance (Mo-S or W-S): d (Å)	3.557	3.560
Intrinsic band gap Δ_0 (eV)	0.86	0.59
Valence band λ_v (eV)	0.215	0.486
Conduction band λ_c (eV)	-0.034	+0.051
Effective mass $m^* = m_e/m_0$	0.655	0.246
Lande factor g_s	2.21	2.84
Lande factor g_v	3.57	4.96
Thickness of the monolayer h(Å)	3.610	3.624
Relative indices $n_r = \sqrt{\epsilon_r}$	4.375	3.173

IV. CONCLUSIONS

In summary, the linear, nonlinear and total AC as well the RI variations in MoTe₂, WTe₂ and their W-composition dependence has been explored in details. Apart from W-concentrations, factors such as inter-band transitions were responsible for the notable changes in their linear and non-linear optical properties. The increase of W-concentration causes a red-shift and reduces or increases the amplitudes of the resonant peaks. The results indicated that, the optical phonon play the same footing role as acoustic photon in inter-band transition. Conclusively, the findings on $W_xMo_{1-x}Te_2$ nano-sheets project it as a suitable material for optoelectronic device applications.

REFERENCES

- [1] G-B Liu et al, Phys. Rev. B 88 (2013) 085433.
- [2] N. Zibouche, A. Kuc, J. Musfeldt, and T. Heine, Ann. Phys. (Berlin) 526, No. 9-10, (2014) 395-401
- [3] C. Ruppert, O. B. Aslan, and T. F. Heinz, Nano Lett. 14 (2014) 6231-6236
- [4] Pavel V. Ratnikov, Phys. Rev. B 102 (2020) 085303
- [5] H. H. Huang, Xiaofeng Fan, David J. Singh, Hong Chen, Q. Jianga and W. T. Zheng, Phys. Chem. 18 (2016) 4086
- [6] Chang TR., Xu SY., Chang G. et al. Nat Commun 7 (2016) 10639.

- [7] Belopolski I., Sanchez D., Ishida Y. et al. *Nat Commun* 7 (2016) 13643
- [8] Jiang C., Liu F., Cuadra J. et al. *Nat Commun* 8 (2017) 802 ; Sean M Oliver et al, *2D Mater.* 4 (2017) 045008.
- [9] K.F. Mak, C. Lee, J. Hone, J. Shan, Tony F. Heinz, *Phys. Rev. Lett.* 105 (2010) 136805.
- [10] H. Zeng, J. Dai, W. Yao, D. Xiao, X. Cui, *Nat. Nanotechnol.* 7 (2012) 490-493.
- [11] H. Huang, J. Zha, S. Li, C. Tan, *Chin. Chem. Lett.* 33 (2022) 163-176.
- [12] Y. ASADI, Z. NOURBAKHSI, *J. Electron. Mater.* 48 (2019) 7977.
- [13] J. He, D. He, Y. Wang, H. Zhao, *Opt. Express* 23(2015) 33370.
- [14] S.Bhoyate, J.Kim, E.Lee, B.Park, E.Lee, J.Park, S.H.Oh, Je.Kim,W.Choi, *J. Mater. Chem. A* 8 (2020) 12436-12445.
- [15] B. Radisavljevic, A. Radenovic, J. Brivio, V. Giacometti, A. Kis, *Nat. Nanotechnol.* 6 (2011) 147-150.
- [16] X. Wang, S. Yang, Q. Yue, F. Wu, J. Li, *J. Alloys Compd.* 615 (2014) 989–993.
- [17] A. Allain, J. Kang, K. Banerjee, A. Kis, *Nat. Mater.* 14 (2015) 1195-1205.
- [18] X.Yin, A. Teng, Z. Chang, P. Yuan, D. Zhang, J. Yu, *Catalysts MDPI*, 12 (2022) 456.
- [19] P.T. Huong, D. Muoi, T.N. Bich, H.V. Phuc, C. Duque, P.T.N.Nguyen, C.V.Nguyen, N.N. Hieu, L. T. Hoa, *Physica E: Low Dimens. Syst. Nanostruct.* 124 (2020) 114315.
- [20] N.D. Hien, C.V. Nguyen, N.N. Hieu, S. Kubakaddi, C. Duque, M.M. Ramos, L. Dinh, T.N. Bich, H.V. Phuc, *Phys. Rev. B* 101 (2020) 045424.
- [21] G. Catarina, J. Have, J. F. Rossier, N. M. Peres, *Phys. Rev. B* 99 (2019) 125405.
- [22] Z. Jilidi, S. Baachaoui, N. Raouaf, S. Ridene, *Int. J. Light Electron Opt.* 228 (2021) 166166.
- [23] S. Ridene, K. Boujdaria, H. Bouchriha, and G. Fishman, *Phys. Rev. B* 64 (2001) 085329.
- [24] G. Rezaei, M. Karimi, A. Keshavarz, *Physica E: Low Dimens. Syst. Nanostruct.* 43 (2010) 475-481.
- [25] L. Li, Z. Xu, Y. Li, X. Zhang, C. Zhang, Y. Ouyang, Y. Jiang, X. Zhuang, and A. Pan, *ACS Appl. Nano Mater.* 6 (2023) 17111 - 171.